•计算机科学与技术•

DOI:10.12454/j.jsuese.202400259

本刊网刊

分布式超声波探测2维气体温度场方法研究

李少壮[1,2],石友安[2*],陆小康[1,2],陈　雨[1],魏　东[2]

(1.四川大学 电子信息学院,四川 成都 610065;2.空天飞行空气动力科学与技术全国重点实验室,四川 绵阳 621000)

摘　要:在现有的热压罐中,设备主要使用若干温度传感器来实现复材构件成型温度控制,但这种点测的方式难以实现空间温度场的测量,同时,这种接触式测温方式会直接影响模具和构件接触面温度分布。这些局限性大大影响了构件成型的品质,准确测量大型空间构件成型气体温度场成为航空复合材料部件成型固化亟需解决的难题。为此,本文开展分布式超声波探测2维气体温度场方法研究。首先,通过数值仿真进行热压罐中的超声传播特性分析研究,并在此基础上依据时移特性建立分布式超声气体测温模型;其次,从热压罐实际工况出发,发展基于全局径向基函数(LQ)和奇异值分解(SVD)的2维气体温度场重建算法(LQ–SVD),并通过和其他几个常见温度场重建算法作对比及带噪重建的方式进行该算法的考核与精度分析。数值模拟和热压罐现场实验表明:当温度场发生变化时,超声在热压罐中的传播会出现明显的时移特性;以该时移特性建立的测温模型可有效描述温度分布变化与超声传播时间的关系;LQ–SVD重建算法在热压罐工况下具有较高精度和抗噪性,在数值模拟中该算法抗噪性较强且和其他算法相比具有更低的重建均方根误差,在实验验证中重建值和真值吻合较好;本文建立的分布式超声波探测2维气体温度场方法可较为准确地测量出大型空间2维气体温度场。

关键词:超声气体测温;分布式;2维气体温度场;温度场重建;径向基函数

中图分类号:TP391.9　　**文献标志码:**A　　**文章编号:**2096-3246(2025)03-0256-11

热压罐工艺是目前先进复合材料构件成型固化的主要制备工艺之一[1–3]。为满足大型构件的高品质制备需求[4],热压罐的直径和长度也须增大。同时,为提高制备效率,还面临多个构件同时成型需求[5]。这些新的需求使得热压罐内部空间对流、导热、辐射、材料固化散热之间耦合加剧,空间环境、模具、构件组成的成型固化温度场测量与控制面临巨大压力,构件成型品质受到严重制约[6–8],如何准确测量大型空间构件成型气体温度场是航空复合材料部件成型固化亟需解决的难题。

目前,主要通过若干温度传感器联网,测量空间环境和模具若干点温度来实现复材构件温度的控制[9–10]。由于该方式测点有限,对于大型空间较难实现瞬态温度场的测量。另外,由于该方式是接触式,较难在不影响模具和构件接触的情况下实现模具接触面温度分布的无损测量[11]。随着构件尺寸增加,这些局限对于成型品质的影响越来越突出。超声测温是一种基于声信号无损测量内部温度分布的新方法,具有非接触、实时和场测量等特点[12–14]。但目前尚缺少热压罐中的分布式超声探测2维气体温度场方法。

为此,本文开展了分布式超声波探测2维气体温度场方法研究。首先,研究热压罐中的超声传播特性,在此基础上建立分布式超声气体测温模型;其次,从热声耦合反问题角度入手,发展基于全局径向基函数(LQ)和奇异值分解(SVD)2维气体温度场重构算法(LQ–SVD),并进行算法的考核与精度分析;最后,通过数值模拟和热压罐现场实验进行方法有效性验证。

1　成型空间气体温度场中超声传播特性

基于超声波建立复材构件成型空间气体温度场感知模型的前提是分析超声波在热压罐中具有怎样的传播特性,以及当温度场变化时声波的变化情况。

收稿日期:2024 – 04 – 14　　**修回日期:**2024 – 07 – 11　　**网络出版日期:**2025 – 03 – 20

基金项目:国家自然科学基金项目(52276168);四川省科技计划项目(2022YFG0051)

作者简介:李少壮(1999—),男,硕士生. 研究方向:超声测温. E-mail:13986948428@163.com

* **通信作者:**石友安,副研究员,E-mail:youanshi11@sina.com

通过数值模拟，首先分析研究稳态温度场条件下热压罐中的超声传播特性，接着进一步分析不同温度场下超声传播特性。

算例中气体区域为直径为 0.1 m 的圆形；换能器压电材料为 PZT–5H；激励信号是频率为 100 kHz 的 3 周期正弦调制高斯脉冲；壁面边界条件为硬声场边界。算例模型如图 1 所示，计算流程如图 2 所示。被测温度场（K）为单峰对称温度场，记为 $T_1(x,y)$，其中，x和y 分别为点的横、纵坐标，该温度场函数表达式如下：

$$T_1(x,y)=500\mathrm{e}^{-\frac{x^2+y^2}{0.5}} \tag{1}$$

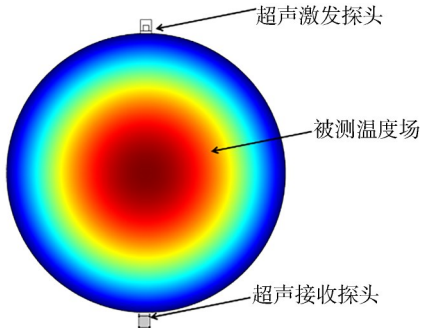

图 1　超声气体测温示意图

Fig. 1　Ultrasonic gas temperature measurement schematic diagram

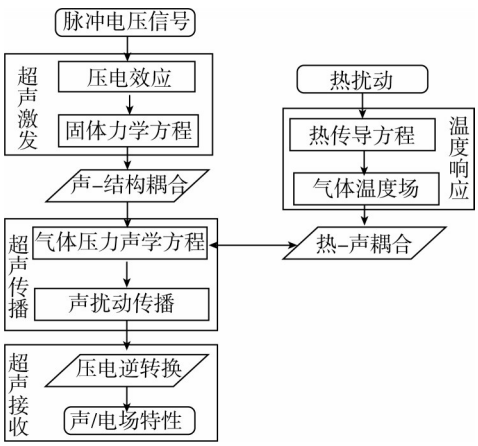

图 2　计算流程

Fig. 2　Calculation process

不同时刻气体空间的声压分布如图 3 所示，接收端随时间的声压变化情况计算结果如图 4 所示。

压电换能器受脉冲电压激发后，因逆压电效应，产生主脉冲纵波，呈辐射状向被测气体介质内部传播，沿程衰减（图 3（a）、（b））；受固壁硬声场边界影响，超声波在壁面发生反射，产生壁面反射纵波（图 3（c））；由于壁面是圆形，随着超声传播的深入，反射角逐渐增大，壁面反射纵波与壁面发生 2 次反射（图 3（d）），产生壁面 2 次反射纵波。当主脉冲纵波传播到接收探头时，由于界面处声阻抗的变化，一部分波透射，一部分波则被反射回来，形成主脉冲反射波。随后，壁面反射纵波相继传播到接收探头，并发生相互干扰，再反射，形成多次壁面反射波（图 3（d）、（e））。反射的主脉冲纵波和壁面波又继续在气体内部传播、衰减、再反射，形成多种 2 次反射波（图 3（f））。波的传播、反射、衰减符合物理规律，表明算法有效。

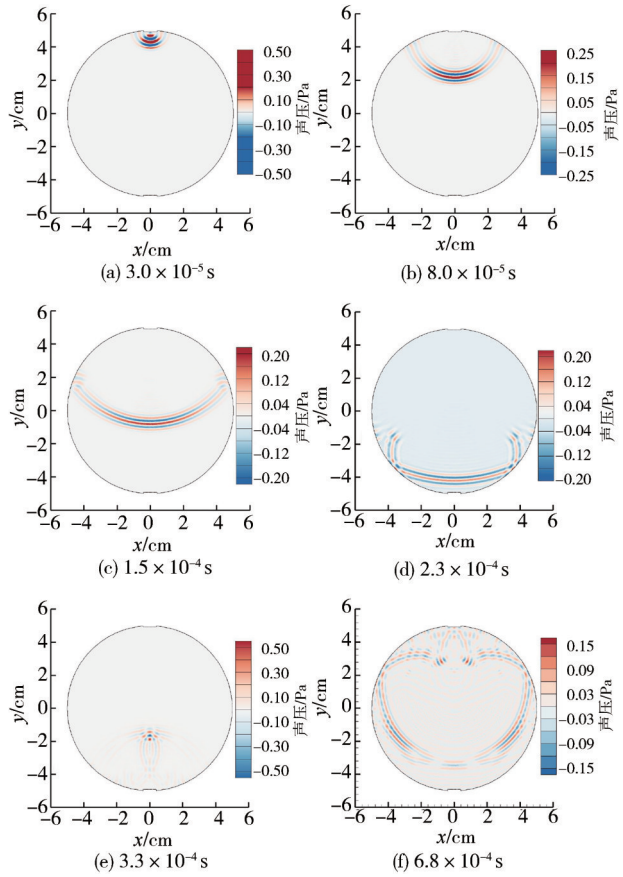

图 3　不同时刻成型气体空间的声压分布

Fig. 3　Sound pressure distribution in the gas space at different times

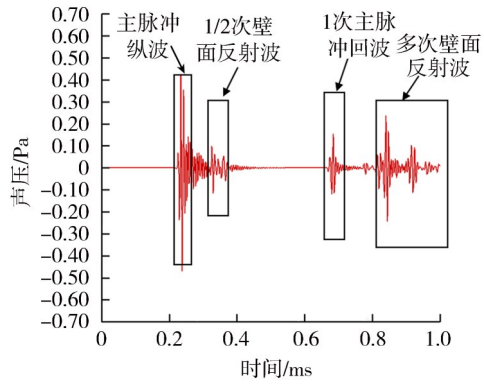

图 4　接收端的声压计算结果

Fig. 4　Calculation results of sound pressure at the receiving end

接着，改变温度场条件，模型仍为单峰对称，分别记为 $T_2(x,y)$ 和 $T_3(x,y)$，函数表达式如下：

$$T_2(x,y)=450\mathrm{e}^{-\frac{x^2+y^2}{0.5}} \quad (2)$$

$$T_3(x,y)=400\mathrm{e}^{-\frac{x^2+y^2}{0.5}} \quad (3)$$

图 5 为不同温度场接收端声压计算结果。由图 5 可知，3 种不同温度场条件下到达接收端的主脉冲纵波存在微秒级的时间差。当热压罐空间温度分布变化时，波速分布发生变化，导致路径上的超声传播时间发生变化，因此，接收端信号会出现“时移特性”。

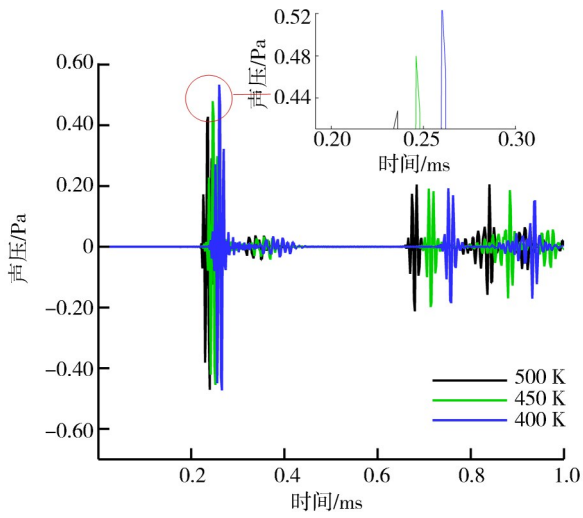

图 5 不同温度场接收端声压计算结果

Fig. 5 Calculation results of sound pressure at the receiving end under different temperature fields

超声波在热压罐内部气体空间的传播中，除主脉冲纵波外，还存在多种反射波及波的相互干扰，传播行为比较复杂。且随着温度分布不同，超声在路径上的传播时间不同，在本算例中“时移特性”为微秒量级，这与介质的物性、温度场以及超声波的传播距离等因素有关。

2 分布式超声气体测温模型

气体介质中的温度分布发生变化时，随着超声波的传播，声能发生衰减，同时声速发生变化声时出现“时移特性”。本质上，超声渡越时间反映了波传播路径上温度分布的累积量。因此，从波速与温度的相关性出发，建立分布式超声波感知气体介质中温度分布变化的分析模型。

对于空间温度场分布的超声探测，本文采用分布式超声探测方案，如图 6 所示。图 6 中，红色的 A1、B1、C1、D1 为 4 个激发换能器，蓝色的 A2、B2、C2、D2 为 4 个接收换能器。方案的核心思想是将被测区域划分为若干个视为温度均匀分布的子温区，通过布设多组声波换能器形成多条声波路径，每条路径都会穿过多个子温区，每个子温区也会被多条路径穿过。通过测量每条路径的超声传播时间，重构出被测区域的完整温度分布。

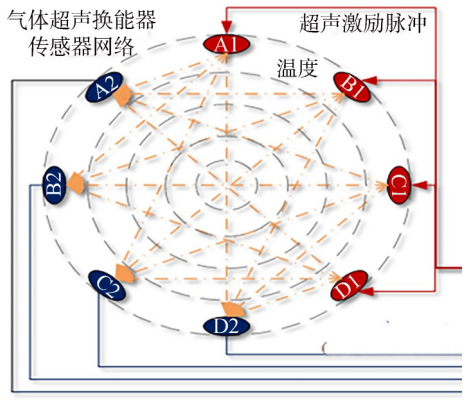

图 6 分布式超声气体测温方案

Fig. 6 Distributed ultrasonic gas temperature measurement scheme

多路超声传播时间 $\{t_{\mathrm{tof}}\}_M$ 描述如下：

$$\{t_{\mathrm{tof}}\}_M=\left\{\int\frac{1}{V\left(T(x,y,t)\right)}\mathrm{d}s\right\}_M \quad (4)$$

式中：M 为超声传播路径数；$\{\cdot\}_M$ 表示公式适用于所有路径，共 M 条；s 为当前传播路径；$V\left(T(x,y,t)\right)$ 为坐标为 (x,y) 的点在时刻 t 的绝对温度 T(K)所决定的超声传播速度。

每个检测周期内，各声波换能器按顺序依次发声，当某个换能器发声时，其余所有换能器接收信号。经过计算机处理分析，得到各条路径的声波飞渡时间，结合温度场重构算法求解出声波的速度分布，最终通过式(5)[15–16]计算出被测区域的温度分布。

$$\begin{cases}V=\sqrt{\gamma RT}=Z\sqrt{T},\\ Z=\sqrt{\gamma R}\end{cases} \quad (5)$$

式中：V 为气体中声波的传播速度，m/s；γ 为气体绝热系数，由气体的物理性质决定；Z 为气体的声音传播常数；R 为气体常数。

3 基于全局径向基函数的温度场重建算法

现有的大多温度场重建算法如代数迭代方法、最小二乘法等，存在离散点数不能大于传播路径数、温度分辨率不高等问题[17–18]，因此，本文使用基于 LQ 和 SVD 的 2 维温度场重建算法(LQ–SVD)。该算法主要思想是先利用 LQ 函数的线性组合对声速的倒数分布进行拟合，建立反演模型；再利用 SVD 解决反演过程中的病态问题，实现模型求解，其重构流程如图 7 所示。

假设被测区域内的声速的倒数分布为连续函数，记为 $f(x,y)$，则区域中第 k 条超声传播路径的声波飞渡时间理论值 t_k 可表示为：

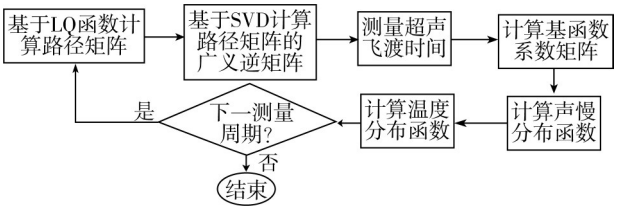

图 7　LQ–SVD 算法重建温度场流程

Fig. 7　LQ–SVD algorithm to reconstruct the temperature field process

$$t_k=\int f(x,y)\mathrm{d}l_k \tag{6}$$

式中，l_k为第 k 条声波传播路径长度。

将被测区域划分为 N 个子温区，$f(x,y)$可表示为 N 个子温区几何中心点径向基函数的线性组合[19]。

$$f(x,y)=\sum_{i=1}^{N}\xi_i\varphi_i(x,y) \tag{7}$$

式中：ξ_i为待定系数；$\varphi_i(x,y)$为第 i 个子温区几何中心点的径向基函数，i=1,2,⋯,N。

2 维 LQ 径向基函数的表达式为：

$$\varphi_i(x,y)=\ln\left(\frac{\delta^2}{\left(x-x_i\right)^2+\left(y-y_i\right)^2+\delta^2}\right) \tag{8}$$

式中：(x_i, y_i)为 LQ 径向基函数的中心，即第 i 个子温区几何中心点的坐标；δ 为基函数形状参数。

联立式(7)和(8)可得：

$$t_k=\sum_{i=1}^{N}\xi_i\int\varphi_i(x,y)\mathrm{d}l_k=\sum_{i=1}^{N}h_{k,i}\xi_i \tag{9}$$

式中，$h_{k,i}$为第 i 个径向基函数在第 k 条路径上的线积分，$h_{k,i}=\int\varphi_i(x,y)\mathrm{d}l_k$。

将式(9)改写为矩阵形式：

$$\boldsymbol{t}=\boldsymbol{H}\boldsymbol{\xi} \tag{10}$$

式中，$\boldsymbol{t}$为 M 条声波路径的飞渡时间构成的矩阵，$\boldsymbol{\xi}$为 M 个径向基函数权重所构成的系数矩阵，$\boldsymbol{H}$为 N 个子温区的 LQ 径向基函数在 M 条声波路径上的积分所构成的路径矩阵。

式(10)的求解是一个不适定问题，多数情况下矩阵 $\boldsymbol{H}$ 为病态矩阵，不存在逆矩阵，但存在伪逆矩阵。对于矩阵 $\boldsymbol{P}$，如果存在一个矩阵 $\boldsymbol{Q}$ 使得二者满足关系 $\boldsymbol{PQP}=\boldsymbol{P}$，$\boldsymbol{QPQ}=\boldsymbol{Q}$，$(\boldsymbol{PQ})^{\mathrm{T}}=\boldsymbol{PQ}$，$(\boldsymbol{QP})^{\mathrm{T}}=\boldsymbol{QP}$，则矩阵 $\boldsymbol{Q}$ 称为矩阵 $\boldsymbol{P}$ 的伪逆矩阵。

SVD[20–21]是处理矩阵病态问题的一种有效手段，它通过提取矩阵的特征向量计算矩阵的伪逆，为矩阵方程提供最优解。大量仿真实验证明了 SVD 在声学测温技术中的有效性[22–23]。

因此，式(10)中待求解的权重矩阵 $\boldsymbol{\xi}$ 可表示为：

$$\boldsymbol{\xi}=\boldsymbol{H}^{+}\boldsymbol{t} \tag{11}$$

式中，$\boldsymbol{H}^{+}$为 $\boldsymbol{H}$ 的伪逆。

将 $\boldsymbol{\xi}$ 代入式(7)并结合式(5)可以得到温度场函数 $T(x,y)$：

$$T(x,y)=\frac{1}{Z^2f^2(x,y)} \tag{12}$$

4　算法考核与精度分析

为了验证 LQ–SVD 算法的重建性能，构造单峰对称、单峰偏置、双峰偏置、三峰偏置以及四峰偏置的典型 2 维温度场，并分析算法对以上 5 种温度场模型的重建精度。另外，通过在飞渡时间模拟真值的基础上叠加不同标准差的高斯白噪声，进行算法抗噪性分析。

图 8 为 2 维温度场声学测量方案示意图。

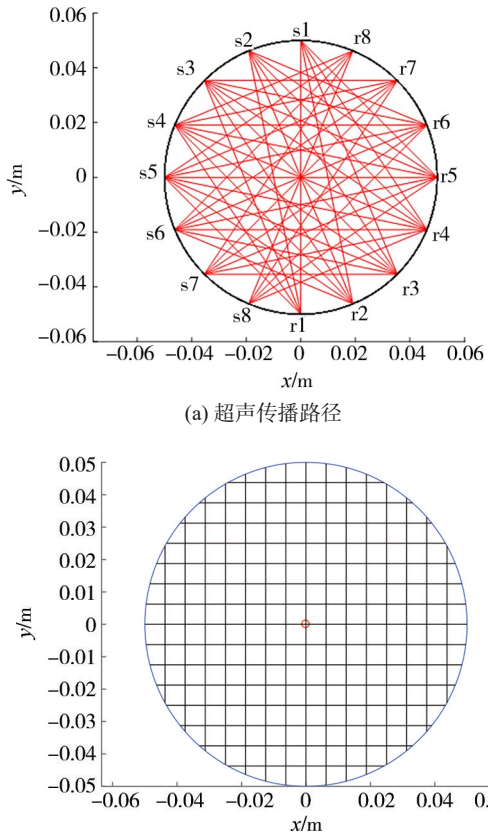

(a) 超声传播路径

(b) 子温区划分

图 8　2 维区域温度场声学测量方案

Fig. 8　Measurement scheme of temperature field in two dimensions

图 8 中：验证算例的被测区域为直径为 0.1 m 的圆形；在测量区域周围均匀地布置了 16 个声波换能器(编号为 s1~r8)；红色实线表示所形成的有效声波传播路径，共 52 条(图 8(a))；测量区域根据其外切正方形等分的共 16×16 个子温区划分了圆内的 172 个子温区(图 8(b))。

以被测区域圆心坐标为原点建立 2 维直角坐标系，各换能器位置如表 1 所示。

表1 2维区域声波换能器位置坐标

Tab. 1 Two-dimensional area acoustic transducer position coordinates

编号	坐标	编号	坐标
s1	(0,0.050)	r1	(0,0.050)
s2	(–0.019,0.046)	r2	(0.019,–0.046)
s3	(–0.035,0.035)	r3	(0.035,–0.035)
s4	(–0.046,0.019)	r4	(0.046,–0.019)
s5	(–0.050,0)	r5	(0.050,0)
s6	(–0.046,–0.019)	r6	(0.046,0.019)
s7	(–0.035,–0.035)	r7	(0.035,0.035)
s8	(–0.019,–0.046)	r8	(0.019,0.046)

在被测区域内分别构造单峰对称、单峰偏置、双峰偏置、三峰偏置以及四峰偏置的典型2维温度场作为仿真重建对象，其函数表达式分别如下。

2维单峰对称温度场函数为 $TM_1(x,y)$：

$$TM_1(x,y)=\frac{5\,000}{2\,600(x^2+y^2)+10} \tag{13}$$

2维单峰偏置温度场函数为 $TM_2(x,y)$：

$$TM_2(x,y)=\frac{5\,000}{800\left((x-0.03)^2+(y-0.03)^2\right)+10} \tag{14}$$

2维双峰偏置温度场函数为 $TM_3(x,y)$：

$$TM_3(x,y)=\frac{1\,900}{1\,900\left((x-0.03)^2+(y-0.03)^2\right)+5}+\frac{2\,000}{1\,800\left((x+0.03)^2+(y+0.02)^2\right)+5} \tag{15}$$

2维三峰偏置温度场函数为 $TM_4(x,y)$：

$$TM_4(x,y)=\frac{1\,700}{3\,500\left((x+0.03)^2+(y+0.03)^2\right)+5}+\frac{1\,600}{4\,000\left((x+0.03)^2+(y-0.03)^2\right)+5}+\frac{1\,850}{3\,300\left((x-0.035)^2+(y-0.02)^2\right)+5} \tag{16}$$

2维四峰偏置温度场函数为 $TM_5(x,y)$：

$$TM_5(x,y)=\frac{700}{3\,000\left((x+0.03)^2+(y+0.03)^2\right)+2}+\frac{750}{3\,000\left((x+0.03)^2+(y-0.03)^2\right)+2}+\frac{750}{3\,000\left((x-0.03)^2+(y-0.03)^2\right)+2}+\frac{700}{3\,000\left((x-0.03)^2+(y+0.03)^2\right)+2} \tag{17}$$

基于上述已知条件，可得到超声传播时间的理论值。然后通过前述LQ–SVD算法进行温度场的重建，重建前后对比结果如图9所示。由图9可以看出：本文所使用的LQ–SVD算法在5个温度场中都具有很好的表现，重建结果与原始温度分布具有较高的一致性。

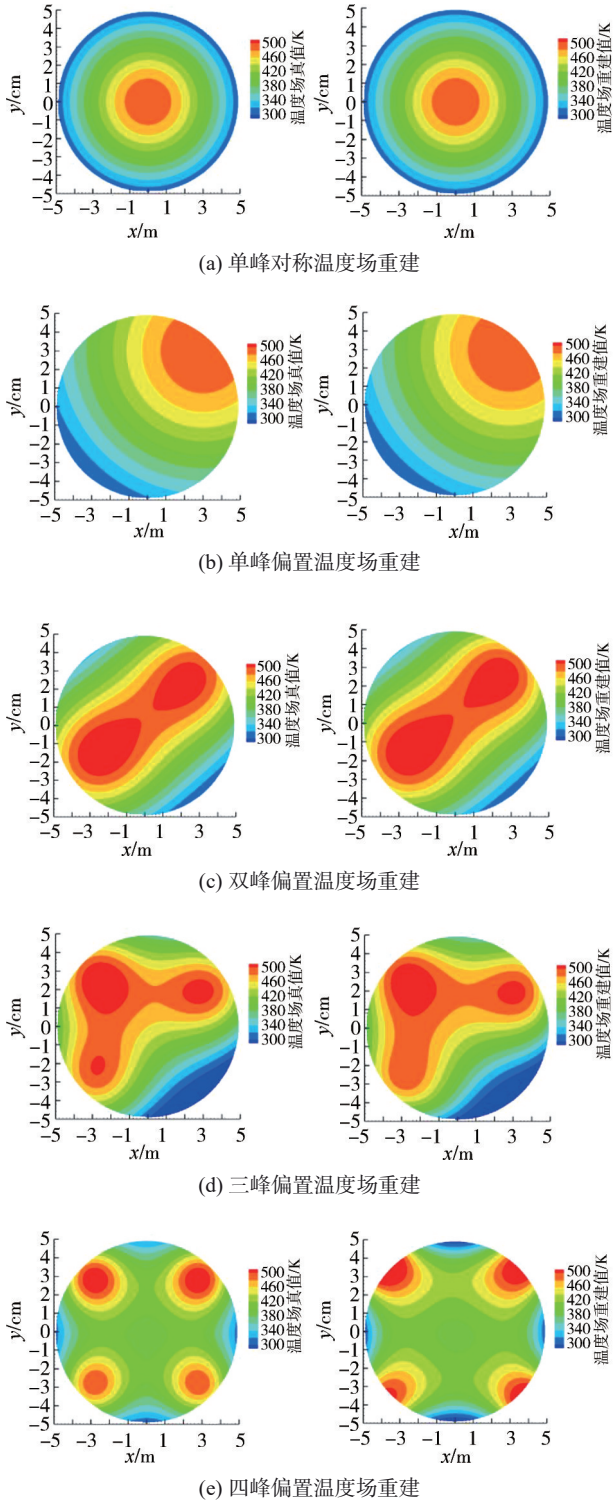

(a) 单峰对称温度场重建

(b) 单峰偏置温度场重建

(c) 双峰偏置温度场重建

(d) 三峰偏置温度场重建

(e) 四峰偏置温度场重建

图9 不同典型2维温度场重建结果

Fig. 9 Reconstruction results of different typical two dimensional temperature fields

为进一步评估不同算法的重建性能，对重建结果进行定量的误差分析。重建误差的评价指标包括最大绝对误差 E_{max}、平均绝对误差 E_{mean} 及均方根误差 E_{rms}，对应的计算公式如下：

$$E_{max}=\max\left|T_j^{R}-T_j^{M}\right| \tag{18}$$

$$E_{mean}=\frac{1}{n}\sum_{i=j}^{n}\left|T_j^{R}-T_j^{M}\right| \tag{19}$$

$$E_{rms}=\frac{\sqrt{\frac{1}{n}\sum_{i=1}^{n}\left(T_j^{R}-T_j^{M}\right)^2}}{T_{mean}^{M}}\times 100\% \tag{20}$$

式(18)~(20)中，n 为被测区域内温度计算点的总个数，T_j^{M} 为第 j 个计算点的仿真温度值，T_j^{R} 为第 j 个计算点的重建温度值，T_{mean}^{M} 为仿真温度场平均温度值。

表 2 为 5 个典型 2 维温度场 3 种重建结果误差。表 3 为 LQ–SVD 算法和马尔可夫径向基法(MK)[24–26]、基于高斯函数的温度场重建算法(GS)[27–28]、基于多 2 次函数的温度场重建算法(MQ)[29–30]3 种常见算法对不同温度场的重建均方根误差对比。由表 2、3 可以看出，LQ–SVD 算法的各项误差指标均较优，有着高度的重建精度。

表 2　2 维温度场重建误差

Tab. 2　Two-dimensional temperature field reconstruction error

温度场	E_{max}/K	E_{mean}/K	E_{rms}/%
单峰对称	0.812 3	0.161 1	0.057 4
单峰偏置	0.043 1	0.008 7	0.002 6
双峰偏置	9.982 9	0.828 3	0.317 5
三峰偏置	16.301 7	2.125 0	0.651 6
四峰偏置	95.163 8	11.184 3	3.878 4

表 3　不同算法重建误差 E_{rms} 对比

Tab. 3　Comparison of reconstruction errors E_{rms} of different algorithms

%

温度场	MQ	MK	GS	LQ–SVD
单峰对称	0.058 3	1.294 0	0.529 1	0.057 4
单峰偏置	0.203 0	0.501 7	0.049 4	0.002 9
双峰偏置	0.588 7	1.220 8	1.800 2	0.317 5
三峰偏置	1.237 8	1.801 7	3.696 5	0.651 6
四峰偏置	3.884 3	3.964 4	10.735 7	3.878 4

进一步对算法进行抗噪性分析。考虑到仿真的工况下温度引起的声时变化最小在 20 us 左右，取 20 us 的 2.5% 和 5.0% 作为高斯白噪声标准差，在模拟真值的基础上分别叠加均值为 0，标准差 σ 为 0.5 us 及 1.0 us 的高斯白噪声，基于带噪声的声时矩阵重建温度场，重建结果和误差分别如图 10 和表 4 所示。从图 10 和表 4 对比可知，在叠加不同程度的噪声之后，重建值与真值仍然吻合较好。

综上可知，本文使用的 LQ–SVD 算法在该工况下具有较好的抗噪性和适用性。

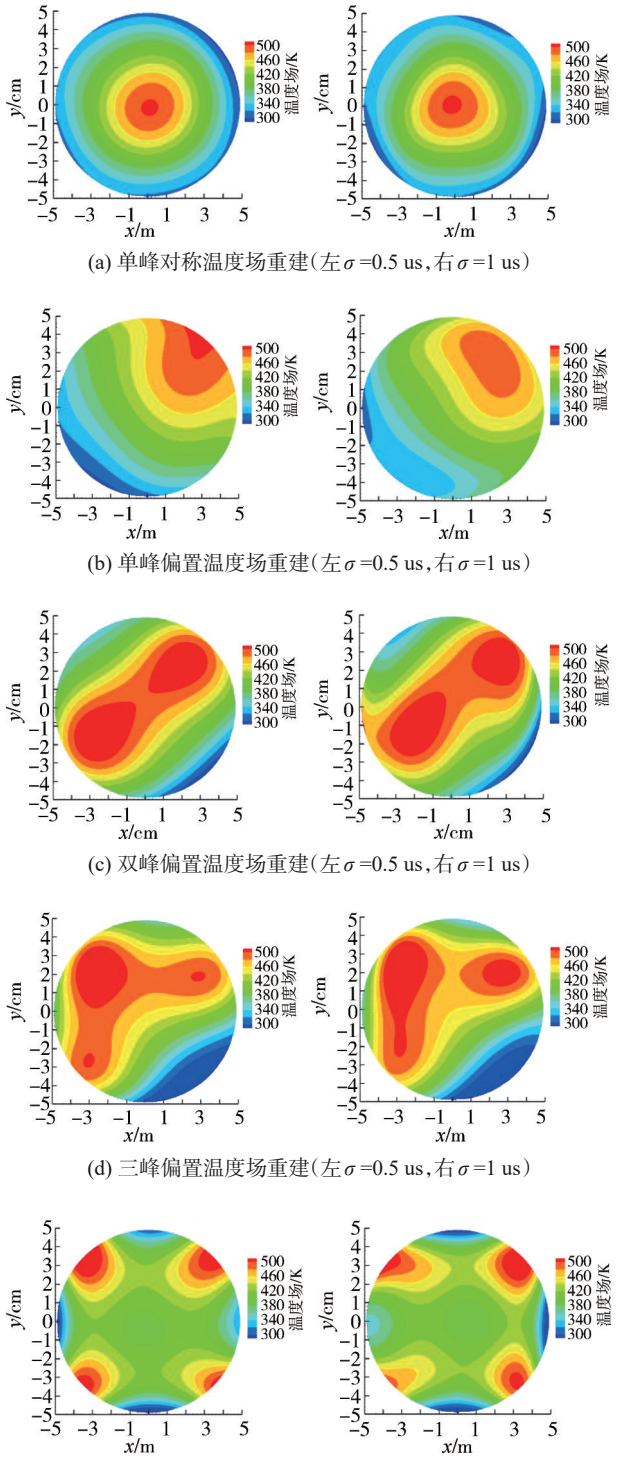

(a) 单峰对称温度场重建(左 σ=0.5 us，右 σ=1 us)

(b) 单峰偏置温度场重建(左 σ=0.5 us，右 σ=1 us)

(c) 双峰偏置温度场重建(左 σ=0.5 us，右 σ=1 us)

(d) 三峰偏置温度场重建(左 σ=0.5 us，右 σ=1 us)

(e) 四峰偏置温度场重建(左 σ=0.5 us，右 σ=1 us)

图 10　不同典型 2 维温度场重建结果

Fig. 10　Reconstruction results of different typical two-dimensional temperature fields

表 4 带噪温度场带噪重建误差

Tab. 4 Noisy temperature field noisy reconstruction errors

重建条件	E_{max}/K	E_{mean}/K	E_{rms}/%
单峰对称,σ=0.5 us	22.409 0	3.965 9	1.338 6
单峰对称,σ=1.0 us	36.578 1	5.779 2	1.956 3
单峰偏置,σ=0.5 us	21.174 7	3.507 9	1.090 3
单峰偏置,σ=1.0 us	46.651 1	7.260 9	2.581 6
双峰偏置,σ=0.5 us	20.757 7	3.417 6	1.051 0
双峰偏置,σ=1.0 us	67.944 5	8.371 8	2.647 0
三峰偏置,σ=0.5 us	25.588 9	4.663 4	1.383 5
三峰偏置,σ=1.0 us	59.341 8	7.221 1	2.333 9
四峰偏置,σ=0.5 us	85.480 4	11.704 6	3.915 8
四峰偏置,σ=1.0 us	90.738 4	14.397 9	4.435 0

5 热压罐超声测温现场验证实验

从实验验证的角度,开展针对热压罐复材构件成型空间气体温度场的分布式超声气体测温实验工作。

实验用热压罐罐体结构及尺寸如图 11 所示。该罐体内径为 60.0 cm,壁厚为 18.7 cm,容积为 0.43 m^3,罐内底部布置了高为 15.0 cm 的架车用于放置构件。

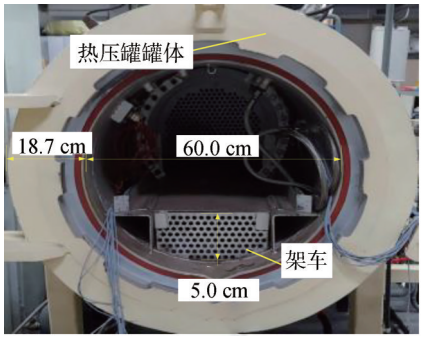

图 11 实验热压罐参数示意图

Fig. 11 Parameter diagram of experimental autoclave

超声测温系统框图和现场布置分别见图 12 和 13。受超声换能器指向性影响,在实测之后采用图 12 中的换能器布局和朝向,以确保每个发射信号(A~J)都能被 10 个接受端捕捉。实验中信号源使用普源信号发生器 DG1000Z 产生频率 40 kHz 的多周期正弦信号;超声换能器选择模块使用的是 16 路串口继电器;换能器型号为 FUS-40E,其谐振频率为 40 kHz,超声信号采集模块使用 NI USB 数据采集卡,热风机作为热源将罐内升温,10 个超声发射换能器和 10 个超声接收换能器组成的阵列共形成了 100 条超声传播路径。分布式超声测温系统现场测量 100 条路径得到的超声飞渡时间经过校准,可以得到如图 14 所示的 100 路超声飞渡时间。

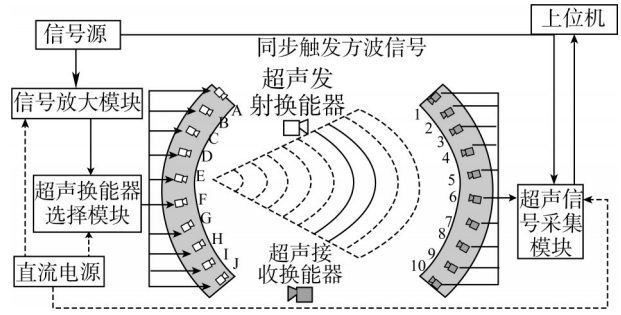

图 12 实验现场示意图

Fig. 12 Experimental site diagram

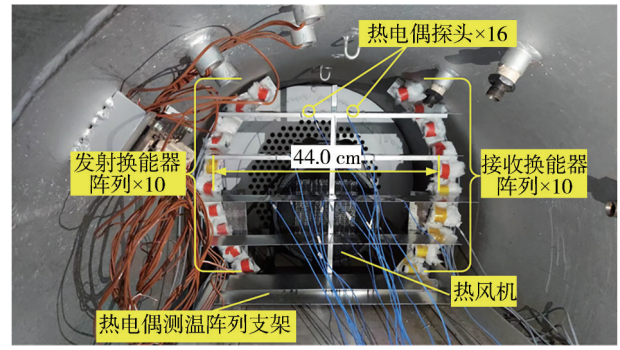

图 13 热压罐超声测温实验现场

Fig. 13 Autoclave ultrasonic temperature test site

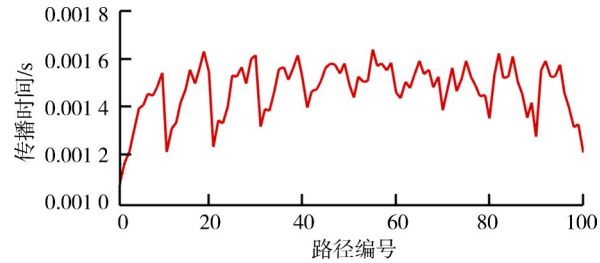

图 14 各路径超声飞渡时间

Fig. 14 Ultrasonic transit time of each path

将 100 路超声飞渡时间输入给 LQ-SVD 重建算法,便可反演出热压罐此时的 2 维温度场分布,如图 15 所示。

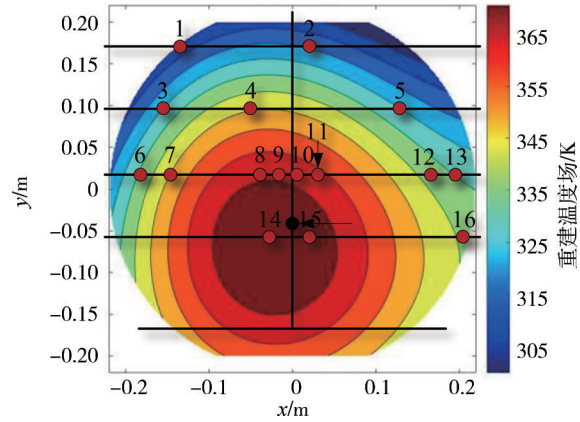

图 15 重建温度场及热电偶阵列的位置

Fig. 15 Reconstruct the location of the temperature field and thermocouple array

图 15 中标注了 16 个热电偶(1~16)在温度场中的位置,表 5 给出了这 16 个温度场真值、重建值及重建的绝对和相对误差。从表 5 可以看出,分布式超声气体测温系统测量出的温度场数据与热电偶测量所得温度趋势基本一致。经计算,重建温度与热电偶测点实测温度的平均相对误差为 4.48%,分布式超声测温系统温度场重建效果良好。

表 5　热电偶实测温度、重建温度及误差

Tab. 5　Measured temperature, reconstructed temperature and error of thermocouple

热电偶编号	热电偶测量温度/℃	重建场温度/℃	绝对误差/℃	相对误差/%
1	89.6	94.85	5.25	5.86
2	94.2	98.85	4.65	4.94
3	96.6	101.85	5.25	5.43
4	94.4	96.85	2.45	2.60
5	91.2	94.85	3.65	4.00
6	88.8	93.85	5.05	5.69
7	97.3	102.85	5.55	5.70
8	98.8	103.85	5.05	5.11
9	98.7	102.85	4.15	4.20
10	99.8	101.85	2.05	2.05
11	94.3	95.85	1.55	1.64
12	89.7	92.85	3.15	3.51
13	94.6	97.85	3.25	3.44
14	94.1	98.85	4.75	5.05
15	90.2	95.85	5.65	6.26
16	87.4	92.85	5.45	6.24

6　结　论

本文针对热压罐成型空间气体温度场测量难题,主要研究了构件成型空间热/声耦合作用下超声波传播特性分析、全局大型温度场重构和分布式多源超声探测等多项关键技术。通过数值模拟和热压罐现场实验验证,得到如下结论。

1)超声波在热压罐中的传播过程中除了会出现主脉冲回波,还会产生较为明显的多次壁面反射;随着空间温度分布不同,接收端信号产生明显的“时移特性”,基于此可建立分布式超声气体测温模型。

2)基于 LQ–SVD 的 2 维温度场重建算法重建的空间温度分布,从云图及具体误差数值看,重建的温度场具有较高的分辨率,精度较高。从时间真值带噪测试结果看,算法抗噪性较好,算法有效。

3)本文建立的分布式超声探测 2 维气体温度场方法可以较为细致地描述热压罐中热声耦合作用下的超声波的传播特性,可以较精确地反演探测出热压罐空间温度场分布,计算的结果符合物理规律,方法有效。

参考文献:

[1] 周益星,向宝林,袁喆,等.复合材料热压罐固化参数在线检测技术研究[J].科技创新与应用,2023,13(11):177–180.

[2] Haskilic V,Ulucan A,Atici K B,et al.A real-world case of autoclave loading and scheduling problems in aerospace composite material production[J].Omega,2023,120:102918.

[3] Wang Yucheng,Tao Fei,Zuo Ying,et al.Digital-twin-enhanced quality prediction for the composite materials[J].Engineering,2023,22:23–33.

[4] Guo Yonggang.Study on numerical simulation of hot-fluid-solid multi-physical field in autoclave forming process[D].Tianjin:Civil Aviation University of China,2022.[郭永刚.热压罐成型工艺的热流固多物理场数值模拟研究[D].天津:中国民航大学,2022.]

[5] Zhang Cheng.Trade-off design of process temperature field of large composite structure autoclave[D].Harbin:Harbin Institute of Technology,2009.[张铖.大型复合材料结构热压罐工艺温度场权衡设计[D].哈尔滨:哈尔滨工业大学,2009.]

[6] Lin Jiaguan,Yang Rui,Wang Tingxia,et al.Large-scale composite curing temperature analysis and improvement in autoclave process[J].Fiber Reinforced Plastics/Composites,2015(5):61–65.[林家冠,杨睿,王廷霞,等.大型复合材料构件热压罐成型温度分析与均匀性改善研究[J].玻璃钢/复合材料,2015(5):61–65.]

[7] Lin Jiaguan.Temperature field analysis and control of curing of composite components in autoclave[D].Dalian:Dalian University of Technology,2015.[林家冠.复合材料构件热压罐固化的温度场分析与调控[D].大连:大连理工大学,2015.]

[8] He Jun,Cao Meng,Cong Fanglin,et al.Research on forming process of aviation composite material based on finite element simulation[J].IOP Conference Series:Earth and Environmental Science,2021,696(1):012015.

[9] Wu Jingwen,Gu Shanlin,Xiong Junfeng,et al.Research on calibration method of autoclave temperature monitoring system based on cluster type compensating wire[J].Metrology & Measurement Technique,2022,49(4):32–35.[吴静文,谷山林,熊军锋,等.基于集束型补偿导线的热压罐温度监控系统校准方法的研究[J].计量与测试技术,2022,49(4):32–35.]

[10] Ma Zhou,Ma Wei,Du Pengfei,et al.Arrangement of sen-

sors for measuring temperature in the test of autoclave[C]// Proceedings of the International Conference on Aerospace System Science and Engineering 2022. Singapore: Springer Nature Singapore,2023:191–201.

[11] Sun Yi. Summary of non-contact temperature measurement technology on solid surface[J]. Science and Technology & Innovation,2024(2):73–76.[孙熠 . 固体表面非接触测温技术综述[J]. 科技与创新,2024(2):73–76.]

[12] Wei Dong, Yang Xiaofeng, Shi Youan, et al. A method for reconstructing two-dimensional surface and internal temperature distributions in structures by ultrasonic measurements[J]. Renewable Energy,2020,150:1108–1117.

[13] Liu Qi, Zhou Bin, Zhang Jianyong, et al. A novel time-of-flight estimation method of acoustic signals for temperature and velocity measurement of gas medium[J]. Experimental Thermal and Fluid Science,2023,140:110759.

[14] Barathula S, Chaitanya S K, Alapati J K, et al. Precise temperature reconstruction in acoustic pyrometry: Impact of domain di-scretization and transceiver count[J]. Applied Thermal Engineering,2024,238:122009.

[15] Ren Siyuan. Reconstruction and experimental study of TSR algorithm for gas temperature field by ultrasonic method [D]. Beijing: North China Electric Power University, 2015. [任思源 . 超声法气体温度场的 TSR 算法重建及实验研究[D]. 北京:华北电力大学,2015.]

[16] Yao Ming lin, Guan Yu jun, Dong Cui ying. Design of ultrasonic gas temperature measurement system with humidity self-correction[J]. Advanced Materials Research,2011,383/384/385/386/387/388/389/390:5166–5170.

[17] Luo Xiaoyu, Liu Piliang, Cui Guimei, et al. Research on reconstruction algorithm of blast furnace throat temperature field[C]//Proceedings of the 2022 6th International Conference on Electronic Information Technology and Computer Engineering. Xiamen: ACM,2022:3573761.

[18] Sheng Xikui, Fang Jianbo, Zhang Xiaohua, et al. Research on temperature field detection method of ultrasonic array reconstruction transformer based on inverse multiquadratic function[C]//Proceedings of 2023 IEEE 5th International Conference on Power, Intelligent Computing and Systems (ICPICS). Shenyang: IEEE,2023:808–813.

[19] Wang Hailin, Zhou Xinzhi, Yang Qingfeng, et al. A reconstruction method of boiler furnace temperature distribution based on acoustic measurement[J]. IEEE Transactions on Instrumentation and Measurement,2021,70:9600413.

[20] Huang Yizhou, Chen Xufei, Badescu E, et al. Adaptive higher-order singular value decomposition clutter filter for ultrafast Doppler imaging of coronary flow under non-negligible tissue motion[J]. Ultrasonics,2024,140:107307.

[21] Wen Dong, Jiao Wenlong, Li Xiaoling, et al. The EEG signals steganography based on wavelet packet transform-singular value decomposition-logistic[J]. Information Sciences,2024,679:121006.

[22] Jia Ruixi, Xiong Qingyu, Xu Guangyu, et al. A method for two-dimensional temperature field distribution reconstruction[J]. Applied Thermal Engineering,2017,111:961–967.

[23] Huang Qunxing, Liu Dong, Wang Fei, et al. Study on three-dimensional flame temperature distribution reconstruction based on truncated singular value decomposition[J]. Acta Physica Sinica,2007,56(11):6742.

[24] Jia Ruixi, Xiong Qingyu, Wang Kai, et al. The study of three-dimensional temperature field distribution reconstruction using ultrasonic thermometry[J]. AIP Advances,2016,6(7):075007.

[25] Shen Xuehua, Xiong Qingyu, Shi Xin, et al. Ultrasonic temperature distribution reconstruction for circular area based on Markov radial basis approximation and singular value decomposition[J]. Ultrasonics,2015,62:174–185.

[26] Shen Xuehua, Xiong Qingyu, Shi Weiren, et al. Temperature distribution monitoring using ultrasonic thermometry based on Markov radial basis function approximation and singular values decomposition[J]. Mathematical Problems in Engineering,2014,2014(1):835619.

[27] Ma Tong, Liu Yuqian, Cao Chengyu, et al. 3D reconstruction of temperature field using Gaussian Radial Basis Functions (GRBF)[C]//Proceedings of 2015 IEEE International Conference on Information and Automation. Lijiang: IEEE,2015:2246–2251.

[28] Ma Tong, Liu Yuqian, Cao Chengyu. Neural networks for 3D temperature field reconstruction via acoustic signals[J]. Mechanical Systems and Signal Processing,2019,126:392–406.

[29] Sun Jian, Wang Ling, Gong Dianxuan. An adaptive selection method for shape parameters in MQ–RBF interpolation for two-dimensional scattered data and its application

to integral equation solving[J].Fractal and Fractional,2023, 7(6):448.

[30] Paul A,Bhattacharya P,Biswas P,et al.Comparative analysis of image deblurring with radial basis functions in artificial neural network[M]//Computational Vision and Robotics.New Delhi:Springer India,2015:135–143.

Study on Distributed Ultrasonic Detection Method of Two-dimensional Gas Temperature Field

LI Shaozhuang[1,2], *SHI Youan*[2*], *LU Xiaokang*[1,2], *CHEN Yu*[1], *WEI Dong*[2]

(1.School of Electronic Information,Sichuan University, Chengdu 610065, China; 2.State Key Laboratory of Aerodynamics, Mianyang 621000, China)

Abstract:

Objective This study applies several temperature sensors in current autoclave systems to control the forming temperature of composite components. This point-measurement method presents challenges in capturing the spatial temperature field. In addition, this contact-based temperature measurement approach directly influences the temperature distribution at the interface between the mold and the components. These limitations significantly affect the quality of component formation. Accurately capturing the gas temperature field during the forming of large-scale spatial components remains a critical challenge in the curing process of aerospace composite material parts. This study investigates a method for distributed ultrasonic detection of the two-dimensional gas temperature field.

Methods This study first employed numerical simulation software to analyze the ultrasonic propagation characteristics in an autoclave under steady-state temperature field conditions from the perspective of thermo-acoustic coupling. The analysis was then extended to ultrasonic propagation characteristics under varying temperature fields. Based on these analyses, a distributed ultrasonic gas temperature measurement model was established using time-of-flight characteristics. In addressing issues associated with inverse problems, such as the limitations of least squares and algebraic iterative methods, where the number of discrete points cannot exceed the number of propagation paths and the temperature resolution is low, a two-dimensional temperature field reconstruction algorithm based on logarithmic-quadratic (LQ) functions and singular value decomposition (SVD) was developed for autoclave conditions. The core idea of this algorithm was to fit the distribution of the reciprocal of sound speed using a linear combination of LQ functions to establish an inversion model. SVD was then employed to address the ill-posedness in the inversion process, which enabled the model to be solved. The accuracy of the LQ–SVD algorithm was analyzed by evaluating the maximum absolute error, mean error, and root mean square error between the reconstructed temperature field and the original temperature field, and the results were compared to those of three other common algorithms. In accounting for practical errors, white noise was added to the theoretical actual values to simulate system errors, and the noise resistance of the algorithm was tested based on this. A distributed ultrasonic temperature measurement system was finally set up in the autoclave for experimental validation. Several thermocouples were utilized to measure the actual temperature field, and the reconstruction error between the experimental system's reconstructed values and the actual values was analyzed to verify the effectiveness of the proposed method.

Results and Discussions In addition to the primary longitudinal wave pulses in the propagation of ultrasound within the gas space of an autoclave, multiple reflection waves and wave interferences were present, resulting in complex propagation behaviors. Due to varying temperature distributions, the propagation time of ultrasound along its path differed. This study examined the “time-of-flight characteristics” at the microsecond level, which were influenced by factors such as medium properties, temperature fields, and the propagation distance of ultrasound. The LQ–SVD algorithm demonstrated the following reconstruction metrics for different types of temperature fields: for a single-peak symmetric temperature field, the maximum absolute error, mean error, and root mean square error were 0.812 3 K, 0.161 1 K, and 0.057 4%, respectively; for a single-peak biased temperature field, these metrics were 0.043 1 K, 0.008 7 K, and 0.002 6%; for a double-peak biased temperature field, they were 9.982 9 K, 0.828 3 K, and 0.317 5%; for a triple-peak biased temperature field, they were 16.301 7 K, 2.125 0 K, and 0.651 6%; and for a quadruple-peak biased temperature field, they were 95.163 8 K, 11.184 3 K, and 3.878 4%. Based on root mean square error, the temperature field reconstruction errors for the Multi-Quadratic (MQ), Markov radial basis function (MK), and Gaussian function-based (GS) algorithms for single-peak symmetric temperature fields were 0.058 3%, 1.249 0%, and 0.529 1%, respectively; for single-peak biased temperature fields, these errors were 0.203 0%, 0.501 7%, and 0.049 4%; for double-peak biased temperature fields, they were 0.588 7%, 1.220 8%, and 1.800 2%; for triple-peak biased temperature fields, they were 1.238 7%, 1.801 7%, and 3.696 5%; and for the quadruple-peak biased temperature fields, they were 3.884 3%, 3.964 4%, and 10.735 7%. These results indicated that regardless of the temperature field model, the LQ–SVD algorithm consistently achieved the best reconstruction performance. In the noise resistance test of the LQ–SVD algorithm, with a noise standard deviation of 0.5 us, the

three reconstruction metrics for single-peak symmetric temperature fields were 22.409 0 K, 3.965 9 K, and 1.338 6%; for single-peak biased temperature fields, they were 21.174 7 K, 3.507 9 K, and 1.090 3%; for double-peak biased temperature fields, they were 20.757 7 K, 3.417 6 K, and 1.051 0%; for triple-peak biased temperature fields, they were 25.588 9 K, 4.663 4 K, and 1.383 5%; and for quadruple-peak biased temperature fields, they were 85.480 4 K, 11.704 6 K, and 3.9158%. With a noise standard deviation of 1 us, these metrics for single-peak symmetric temperature fields were 36.578 1 K, 5.779 2 K, and 1.956 3%; for single-peak biased temperature fields, they were 46.651 1 K, 7.260 9 K, and 2.581 6%; for double-peak biased temperature fields, they were 67.944 5 K, 8.371 8 K, and 2.647 0%; for triple-peak biased temperature fields, they were 59.341 8 K, 7.221 1 K, and 2.333 9%; and for quadruple-peak biased temperature fields, they were 90.738 4 K, 14.397 9 K, and 4.435 0%. In the on-site experimental validation within the autoclave, the average relative error between reconstructed temperatures and thermocouple measurements was 4.48%, which indicated the effective performance of the distributed ultrasound temperature measurement system in temperature field reconstruction.

Conclusions The results demonstrate that the method established in this study for distributed ultrasound detection of two-dimensional gas temperature fields precisely describes the propagation characteristics of ultrasound under thermal/acoustic coupling effects within the autoclave. This method accurately reconstructs the temperature field distribution in the autoclave space. Its effectiveness significantly alleviates the current limitation of relying solely on a few sensor points for temperature measurement in autoclaves. It preliminarily fulfills the requirement for accurate measurement of the temperature field of forming gas in significant spatial components during the molding and curing of aerospace composite material parts, providing robust support for enhancing the quality of component formation in the future.

Key words: ultrasonic gas temperature measurement; distributed; temperature field reconstruction; thermoacoustic coupling; radial basis function

（编辑　吴芝明）

引用格式:Li Shaozhuang,Shi Youan,Lu Xiaokang,et al.Study on distributed ultrasonic detection method of two-dimensional gas temperature field[J].Advanced Engineering Sciences,2025,57(3):256–266.[李少壮,石友安,陆小康,等.分布式超声波探测2维气体温度场方法研究[J].工程科学与技术,2025,57(3):256–266.]